Geology

A mechanism to explain rift-basin subsidence and stratigraphic patterns through fault-array evolution

Sanjeev Gupta, Patience A. Cowie, Nancye H. Dawers and John R. Underhill

Geology 1998;26;595-598
doi: 10.1130/0091-7613(1998)026<0595:AMTERB>2.3.CO;2

Notes

A mechanism to explain rift-basin subsidence and stratigraphic patterns through fault-array evolution

Sanjeev Gupta*
Patience A. Cowie
Nancye H. Dawers
John R. Underhill
Department of Geology and Geophysics, University of Edinburgh, West Mains Road, Edinburgh EH9 3JW, United Kingdom

ABSTRACT

Rift-basin stratigraphy commonly records an early stage of slow subsidence followed by an abrupt increase in subsidence rate. The physical basis for this transition is not well understood, although an increase in extension rate is commonly implied. Here, a numerical fault-growth model is used to investigate the influence of segment linkage on fault-displacement-rate patterns along an evolving normal fault array. The linkage process we describe is controlled by a stress feedback mechanism, which leads to enhanced growth of optimally positioned faults. Model results indicate that, even with constant extension rates, slow displacement rates prevail during an initial phase of distributed extension, followed by an increase in displacement rates as strain becomes localized on linked fault arrays. This is due to the dynamics of fault interactions rather than mechanical weakening. Comparison of model simulations with rift-basin subsidence and stratigraphic patterns in the Gulf of Suez and North Sea suggests that the occurrence and timing of rapid basin deepening can be explained by the mechanics of fault-zone evolution, without invoking a change in regional extension rates.

INTRODUCTION

The stratigraphy of many continental rift basins shows a vertical transition from an early fluvial, shallow lake, or shallow-marine succession to a deep lake or deep-marine succession (Lambiase and Bosworth, 1995). Prosser (1993) termed these two stages in rift-basin development the "rift initiation" when the rate of fault displacement is relatively low and sedimentation keeps pace with subsidence, and the "rift climax" when the rate of fault displacement increases markedly and sedimentation cannot keep pace with subsidence. The transition from rift initiation to rift climax is evident in subsidence data for synrift successions, such as the Miocene Gulf of Suez rift (Fig. 1; Steckler et al., 1988). The mechanism for this transition from slow to rapid subsidence is not well understood, although an increase in extension rate is commonly implied (Steckler et al., 1988; Prosser, 1993; ter Voorde et al., 1997).

The formation and filling of extensional basins are controlled by the development of large normal fault systems (Schlische, 1991; Schlische and Anders, 1996). Contreras et al. (1997) applied a self-similar fault-growth model to investigate half-graben evolution using a single fault segment with a constant extensional strain rate. Although their model is able to reproduce overall basin shallowing observed during the rift climax to late synrift and/or postrift succession, it does not explain the rift initiation to rift climax succession. Recent studies of normal fault growth have shown that large fault systems form by the linkage of shorter fault segments (Dawers and Anders, 1995; Cartwright et al., 1995). In this paper, we investigate the influence of fault interaction and linkage during fault-zone evolution on subsidence and stratigraphic patterns in rift basins. We use a numerical model to simulate evolution of a fault array, and then examine the patterns of displacement-rate variation through time along the array. Because the displacement rate is a proxy for the rate of hanging-wall subsidence, these patterns can be compared with stratigraphic and subsidence observations from rift basins.

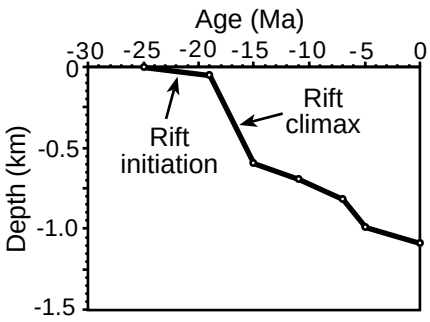

Figure 1. Backstripped tectonic subsidence curve for El Morgan 8 well, Suez rift. Note initial slow rate of tectonic subsidence (rift initiation) followed by abrupt increase in subsidence rate (rift climax).

NUMERICAL MODEL OF FAULT GROWTH

Rupture of an upper-crustal fault results in an elastic strain perturbation in the surrounding rock volume characterized by regions where the stress level is either increased (enhancement zones) or relaxed (shadow zones) (Fig. 2; King et al., 1994). Nearby faults may be brought closer to failure or partially unloaded depending on their location and orientation relative to the rupture zone, hence stress feedbacks are likely to develop in the evolving fault network (Cowie, in press). Positive feedback develops between faults that have mutually overlapping stress enhancement zones, and these faults will grow more rapidly. Negative feedback develops between faults with mutually overlapping shadow zones, resulting in cessation of fault activity. The symmetry properties of the stress perturbation around normal faults will favor the development of en echelon or coplanar fault arrays. In contrast, stress shadow zones develop in the immediate footwall and hanging-wall areas, thereby suppressing adjacent fault growth (Ackermann and Schlische, 1997).

We use the Cowie et al. (1993) thin-plate model for elastic-brittle deformation of a lithospheric plate to demonstrate how stress feedback

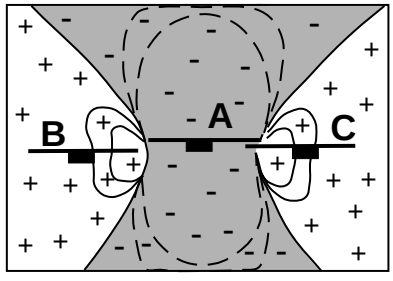

Figure 2. Coulomb stress changes due to slip on a 60° dipping normal fault (A), which enhances (+) or relaxes (–) stress on nearby normal faults (B and C) having same dip and strike (modified from Hodgkinson et al., 1996).

*E-mail: sgupta@glg.ed.ac.uk.

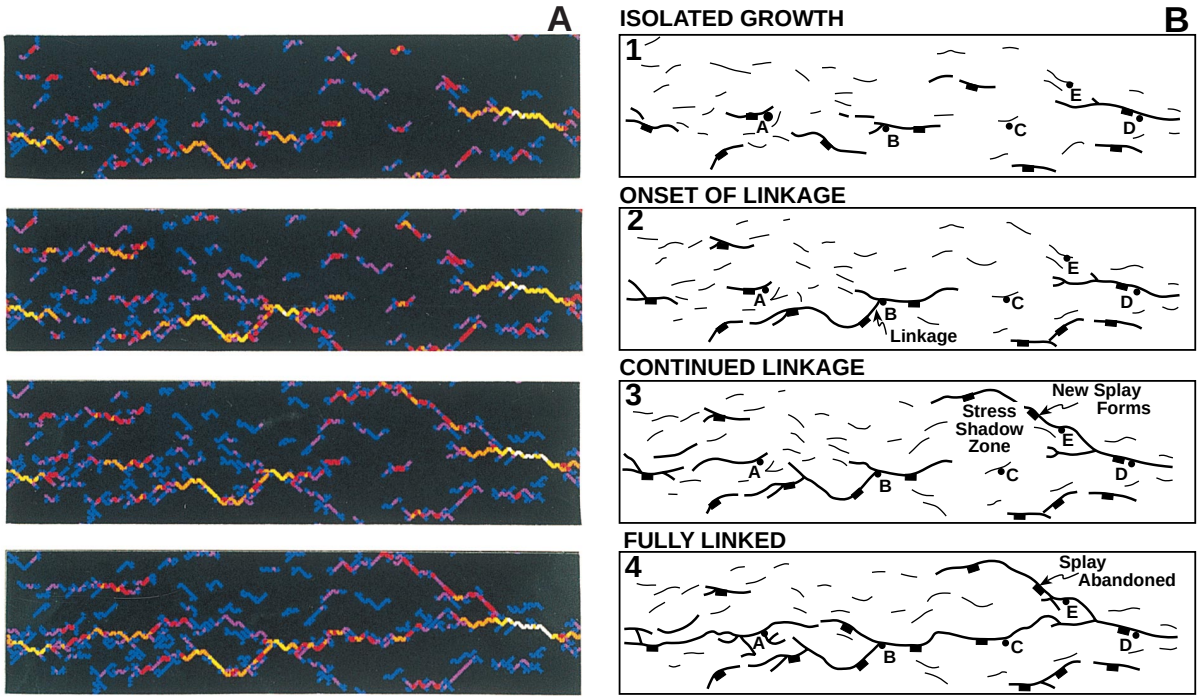

Figure 3. Fault-pattern evolution observed in numerical rupture model at four successive points in time. A: Map of broken lattice elements; accumulated displacement is indicated by normalized color scale (black = unfaulted areas; blue = minimum displacement; white = maximum displacement value at each time step). Each panel shows only central portion of square lattice of 180 × 180 elements. Stress drop at rupture is a proportion of strength of element. Applied strain rate is 2×10^{-9} yr^{-1} across 200-km-wide square plate. B: Schematic fault-evolution maps derived from A using clustering criterion to define trace lengths. Stress field calculation, model scaling, and clustering definition are in Cowie et al. (1993).

between adjacent faults controls fault linkage and variations in displacement rates. Their model consists of a horizontal square lattice with heterogeneous material properties, which do not weaken with time. A constant antiplane shear strain rate is applied across the plate, and cyclic boundary conditions are set along the lateral edges. Coupling between the elastic-brittle lithosphere and underlying ductile layers is not considered in the model. The deformation produced consists of vertical shear dislocations, which accumulate displacement by repeated rupture. Comparison of this model with extensional settings requires an additional rigid-body rotation to produce a series of "domino" fault blocks. Stress changes are calculated throughout the lattice after each rupture event. The pattern of stress enhancement and reduction due to a vertical shear dislocation is comparable to a steeply dipping normal fault (≥60°) in terms of the overall shape and location of the stress perturbations (Fig. 2; Cowie, 1998). The model is strictly applicable only to small amounts of total strain (<5%). The effects of sediment loading and flexural isostasy are not considered, but will only modify the amplitude of the faulted topography produced.

MODEL RESULTS

The evolution of faulting in one of the numerical simulations is shown in Figure 3. At time 1, during the early stages of fault development, several isolated faults of comparable length have formed and weakly interact. Time 2 corresponds to the onset of segment linkage, which takes place as faults interact more strongly. The fault on which B is located more than doubles in length during this time period. Displacement accumulation rates at points B and D show a gradual increase between times 1 and 2 as a consequence of their location near the center of a large fault (D) or due to linkage (B) (Figs. 3, 4). In contrast, points A, C, and E are characterized by slow displacement rates because they are located on faults that are still relatively isolated during times 1 and 2. Between times 2 and 3, the displacement at points A, D, and E increases abruptly because the segments on which they are located have grown substantially by linkage. As linkage progresses, the stress shadows of larger structures result in cessation of fault growth in both the footwall and hanging wall. Consequently, displacement rates increase on the remaining active structures (B, C, and D) to accommodate the imposed constant strain rate (Fig. 4). Point A shows a more gradual transition to a high displacement rate because it is located in a complex zone where the deformation is initially accommodated by two fault strands before localizing onto one. By time 4 the bulk of the strain is accommodated along a narrow zone connecting A, B, C, and D. The overall transition—from slow displacement rates during the early phase of fault development, to more rapid rates as the deformation localizes—begins prior to the formation of a fully linked fault system (Fig. 4).

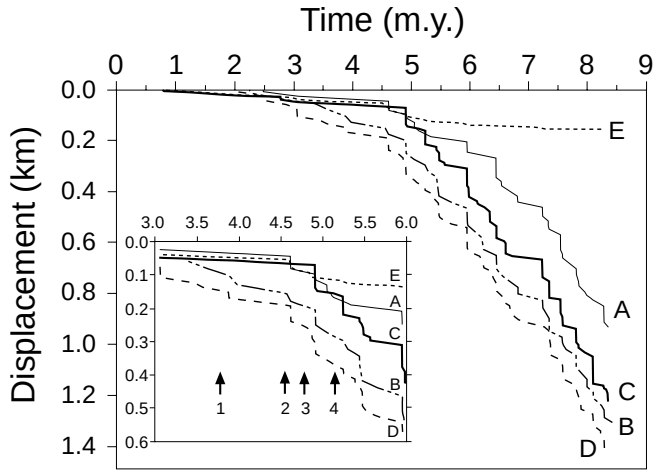

Figure 4. Accumulation of fault displacement as function of time at five points (A–E) along fault array in Figure 3. Note early phase of slow displacement accumulation, which is followed by abrupt increase in displacement rate after 4.5 m.y. Inset shows expanded view of displacement history between 3.0 and 6.0 m.y. Times 1–4 in fault evolution shown in Figure 3 are indicated.

Comparison of behavior at points C and E illustrates the stress feedback mechanism most clearly. At time 3, the fault on which C is located remains isolated and develops very slowly because it lies in the stress shadow zone of the fault on which E is located. Eventually, C begins to undergo positive stress feedback due to its along-strike position from other active segments, whereas the fault on which E is located becomes less optimally positioned within the overall developing structure. Displacement at C starts to increase dramatically when displacement at E switches off because the fault splay on which it lies becomes abandoned.

IMPLICATIONS FOR THE STRATIGRAPHIC DEVELOPMENT OF RIFT BASINS

Our numerical simulation shows that fault interactions during the development of a linked fault system are likely to have a major impact on fault displacement rates, and hence rates of hanging-wall subsidence. Consequently, it should be possible to observe the first-order effects of such fault interactions in the stratigraphic record.

Rift Initiation to Rift Climax Transition

In the Miocene Gulf of Suez rift, fluvial and shallow-marine rift-initiation deposits of the Aquitanian Nukhul Formation are overlain by deep-marine rift-climax deposits of the Burdigalian Rudeis Formation (Patton et al., 1994). Backstripped tectonic subsidence curves throughout the Suez rift indicate that initially, during Nukhul Formation deposition, subsidence rates were low (Fig. 1; Steckler et al., 1988; Richardson and Arthur, 1988). However, between 19 and 21 Ma, there was an abrupt increase in the rate of tectonic subsidence, resulting in the development of a deep-marine basin. We propose that the slow rate of subsidence during the rift initiation stage is a consequence of displacement being distributed on numerous small faults (time 1, Figs. 3, 4). This explains the occurrence of the Nukhul Formation only in isolated subbasins (Richardson and Arthur, 1988). The abrupt transition to high rates of subsidence and the onset of rapid basin deepening during the rift climax may be attributed to fault localization as a consequence of the stress feedback mechanism (times 2 and 3, Figs. 3, 4). Importantly, an increase in regional extension rate is not required to explain this transition, as implied in previous studies (Steckler et al., 1988; Patton et al., 1994).

Development of Sedimentary Depocenters

The numerical simulation indicates that fault interactions occurring prior to the formation of a fully linked fault structure exert a marked control on spatial and temporal variations in displacement rate. Evidence of this comes from seismic interpretations of early rift climax stratal packages in a Late Jurassic half graben located in the northern North Sea rift (Fig. 5A; Dawers et al., 1998). Mapping of the geometry of the Statfjord East fault and thickness distribution of hanging-wall marine-shale successions permits reconstruction of the evolution of sedimentary depocenters in relation to fault activity. During the Bathonian–late Oxfordian, sediment accumulation was localized along the southern part of the Statfjord East fault (Fig. 5B). The Heather Formation shows greatest thickness in the immediate hanging wall of the southwestern segment of the Statfjord East fault. Individual fault segments clearly control the location of subbasin depocenters. With time, displacement propagated toward the northeast (Fig. 5C). Isopachs of the upper Oxfordian–Kimmeridgian lower Draupne Formation indicate continued subsidence along the southern part of the fault, together with development of a new depocenter along a fault segment toward the northeast. We suggest that deposition of the Heather and lower Draupne Formations occurred during a phase of ongoing linkage of fault segments (time 3 in Figs. 3, 4) prior to the development of a fully linked array.

Localization of Fault Activity

Our model predicts that the rift initiation to rift climax transition is related to a combination of enhanced fault linkage and cessation of activity on faults in stress shadow zones. The Upper Jurassic to Lower Cretaceous synrift succession in the Inner Moray Firth basin, North Sea rift, is characterized by marked stratigraphic thickening across normal faults, such as the Smith Bank fault (Fig. 6). Seismic stratigraphic analysis allows its subdivision into six sequences (J1b, J2.1–J2.5, Fig. 6; Underhill, 1991a, 1991b). The earliest synrift sequences (J1b, J2.1 and J2.2) are dissected by numer-

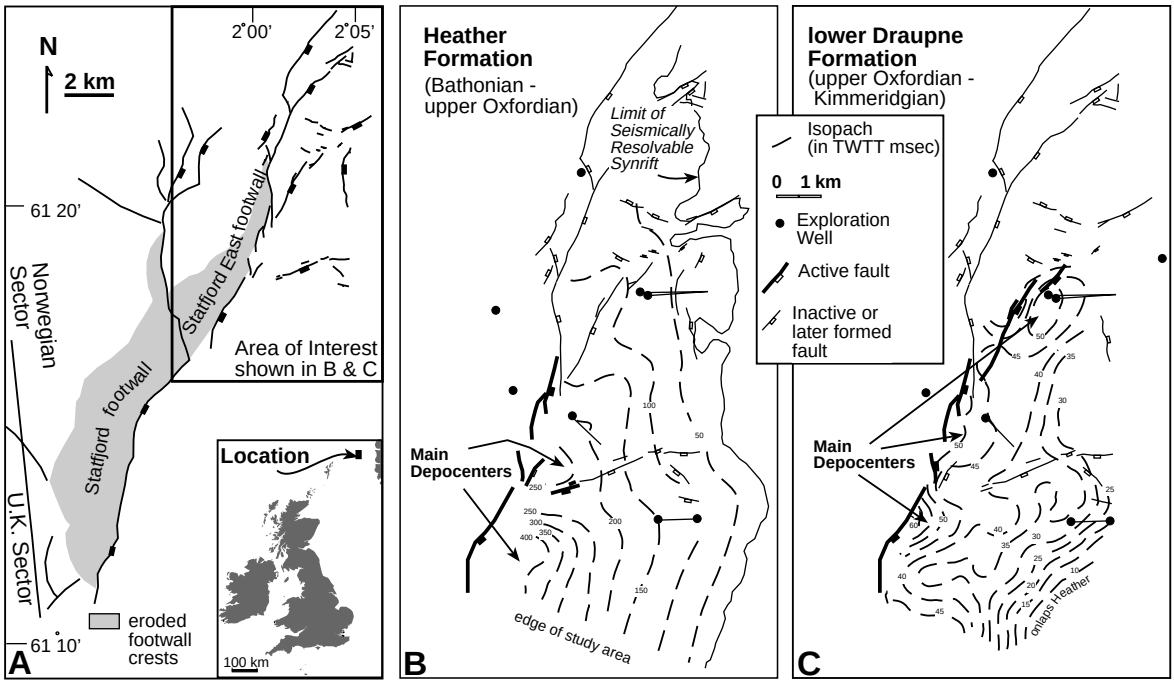

Figure 5. Thickness variation (in two-way traveltime [TWTT] from three-dimensional seismic data) of Upper Jurassic rift climax shale successions in Statfjord East area, northern North Sea. A: Location and overall geometry of Statfjord and Statfjord East faults. Area of interest is hanging wall of Statfjord East fault. B: Thickness variation in Heather Formation. C: Thickness variation in lower Draupne Formation. Fault segments that control thickness variation are shown as bold lines; faults at northernmost tip either had not yet formed or were relatively inactive during Heather and lower Draupne deposi-

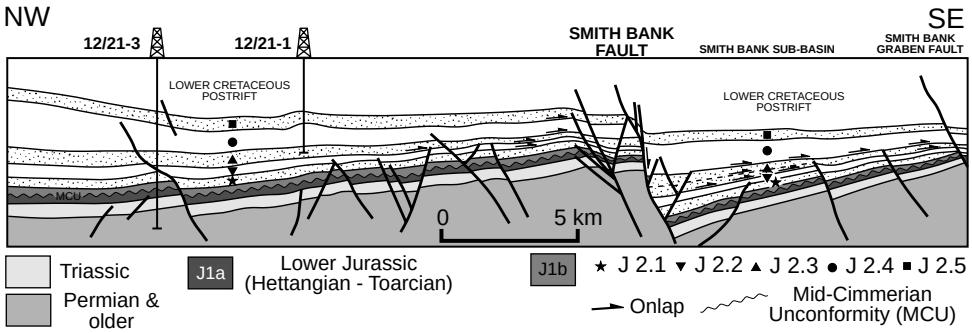

Figure 6. Interpreted seismic line, Inner Moray Firth basin, North Sea, showing Upper Jurassic synrift stratal geometries. Synrift succession is subdivided into six seismic sequences (J1b, J2.1–J2.5). Lowermost sequences (J1b, Bajocian–middle Oxfordian; J2.1–J2.2, upper Oxfordian–lower Kimmeridgian) are dissected by numerous small faults, whereas subsequent sequences (e.g., J2.3, lower-upper Kimmeridgian) show stratigraphic expansion adjacent to a few large faults such as Smith Bank fault.

ous small faults. Later sequences (J2.3 and J2.4) are only affected by a few large faults and show pronounced expansion into their hanging wall and onlap onto the hanging-wall dip slope (Fig. 6). Cessation of activity on smaller faults corresponds to the onset of major displacement accumulation on large faults, such as the Smith Bank fault (J2.3, early–late Kimmeridgian). It is clear that with continued extension, displacement became localized on a few, large, long-lived faults, while other faults became inactive, as demonstrated in our model (point E in Fig. 3).

CONCLUSIONS

Our model leads to a plausible physical explanation for the stratigraphy of many rift basins in that it provides a mechanism for the transition from initially slow rates of subsidence during the rift initiation, to high rates of subsidence during the rift climax. The mechanism depends on stress feedback between interacting faults. The rate of hanging-wall subsidence is found to depend on (1) relative position along a fault segment, (2) proximity and optimal positioning with respect to adjacent fault segments, and (3) occurrence of linkage events. We find that linkage continues after the transition to rift climax is observed. We also find that neighboring faults can have different displacement rates during this transition, consistent with the observations of Nicol et al. (1997). Some authors have invoked variable stretching rates to explain observed synrift stratal geometries (Ravnås and Bondevik, 1997; ter Voorde et al., 1997). Our results suggest that these effects can be explained simply in terms of fault-array evolution at a constant extension rate, and that variable fault activity is an inherent feature of the linkage process.

The assumption of a stress-free boundary at the asthenosphere-lithosphere interface in our model is clearly overly simplistic. Heimpel and Olson (1996) showed that coupling between the elastic-brittle lithosphere and an underlying high-viscosity layer inhibits strain localization and suppresses fault linkage in the upper layer. Nevertheless, good agreement between our observations and model results suggests that viscous effects may be of secondary importance at the strain rates of typical rifts (10^{-16} s^{-1}).

ACKNOWLEDGMENTS

Supported by Marathon Oil (Gupta), The Royal Society of London (Cowie), Natural Environment Research Council (ROPA award GR3/R9521), and Norsk Hydro (Dawers and Underhill). Statfjord East area data provided by Norsk Hydro. We thank M. Steckler for Suez subsidence data, R. Schlische and R. Ackermann for useful comments, and T. Blenkinsop and C. Scholz for critical reviews.

REFERENCES CITED

Ackermann, R. V., and Schlische, R. W., 1997, Anticlustering of small normal faults around larger faults: Geology, v. 25, p. 1127–1130.

Cartwright, J. A., Trudgill, B. D., and Mansfield, C. S., 1995, Fault growth by segment linkage: An explanation for scatter in maximum displacement and trace length data from the Canyonlands Grabens of SE Utah: Journal of Structural Geology, v. 17, p. 1319–1326.

Contreras, J., Scholz, C. H., and King, G. C. P., 1997, A model of rift basin evolution constrained by first-order stratigraphic observations: Journal of Geophysical Research, v. B102, p. 7673–7690.

Cowie, P. A., 1998, A healing-reloading feedback control on the growth rate of seismogenic faults: Journal of Structural Geology (in press).

Cowie, P. A., Sornette, D., and Vanneste, C., 1993, Statistical physics model for the spatiotemporal evolution of faults: Journal of Geophysical Research, v. B98, p. 21809–21821.

Dawers, N. H., and Anders, M. H., 1995, Displacement-length scaling and fault linkage: Journal of Structural Geology, v. 17, p. 607–614.

Dawers, N. H., Berge, A. M., Häger, K.-O., Puigdefábregas, C., and Underhill, J. R., 1998, Controls on Late Jurassic, subtle sand distribution in the Northern North Sea, *in* Boldy, S. A. R., ed., Petroleum geology of NW Europe: Proceedings, Conference of the Geological Society, London, 5th (in press).

Heimpel, M., and Olson, P., 1996, A seismodynamical model of lithospheric deformation: Development of continental and oceanic rift networks: Journal of Geophysical Research, v. B101, p. 16155–16176.

Hodgkinson, K. M., Stein, R. S., and King, G. C. P., 1996, The 1954 Rainbow Mountain–Fairview Peak–Dixie Valley earthquakes: A triggered normal faulting sequence: Journal of Geophysical Research, v. B101, p. 25459–25471.

King, G. C. P., Stein, R. S., and Lin, J., 1994, Static stress changes and the triggering of earthquakes: Seismological Society of America Bulletin, v. 84, p. 935–953.

Lambiase, J. J., and Bosworth, W., 1995, Structural controls on sedimentation in continental rifts, *in* Lambiase, J. J., ed., Hydrocarbon habitat in rift basins: Geological Society [London] Special Publication 80, p. 117–144.

Nicol, A., Walsh, J. J., Watterson, J., and Underhill, J. R., 1997, Displacement rates of normal faults: Nature, v. 390, p. 157–159.

Patton, T. L., Moustafa, A. R., Nelson, R. A., and Abdine, S. A., 1994, Tectonic evolution and structural setting of the Suez Rift, *in* Landon, S. M., ed., Interior rift basins: American Association of Petroleum Geologists Memoir 59, p. 9–55.

Prosser, S., 1993, Rift-related linked depositional systems and their seismic expression, *in* Williams, G. D., and Dobb, A., eds., Tectonics and seismic sequence stratigraphy: Geological Society [London] Special Publication 71, p. 117–144.

Ravnås, R., and Bondevik, K., 1997, Architecture and controls on Bathonian-Kimmeridgian shallow-marine synrift wedges of the Oseberg-Brage area, northern North Sea: Basin Research, v. 9, p. 197–226.

Richardson, M., and Arthur, M. A., 1988, The Gulf of Suez–northern Red Sea Neogene rift: A quantitative basin analysis: Marine and Petroleum Geology, v. 5, p. 247–270.

Schlische, R. W., 1991, Half-graben basin filling models: New constraints on continental extensional basin development: Basin Research, v. 3, p. 123–141.

Schlische, R. W., and Anders, M. H., 1996, Stratigraphic effects and tectonic implications of the growth of normal faults and extensional basins, *in* Beratan, K. K., ed., Reconstructing the structural history of Basin and Range extension using sedimentology and stratigraphy: Geological Society of America Special Paper 303, p. 183–203.

Steckler, M. S., Berthelot, F., Lyberis, N., and LePichon, X., 1988, Subsidence in the Gulf of Suez: Implications for rifting and plate kinematics: Tectonophysics, v. 153, p. 249–270.

ter Voorde, M., Ravnås, R., Færseth, R., and Cloetingh, S., 1997, Tectonic modelling of the Middle Jurassic synrift stratigraphy in the Oseberg-Brage area, northern Viking Graben: Basin Research, v. 9, p. 133–150.

Underhill, J. R., 1991a, Implications of Mesozoic-recent basin development in the western Inner Moray Firth, UK: Marine and Petroleum Geology, v. 8, p. 359–369.

Underhill, J. R., 1991b, Controls on Late Jurassic seismic sequences, Inner Moray Firth, UK North Sea: A critical test of a key segment of Exxon's original global cycle chart: Basin Research, v. 3, p. 79–98.

Manuscript received January 12, 1998
Revised manuscript received April 20, 1998
Manuscript accepted April 24, 1998